Macromolecules

ARTICLE

pubs.acs.org/Macromolecules

Solvent Effects on Template Wetting Nanofabrication of MEH-PPV Nanotubules

Steven D. Bearden,[†] Joseph P. Cannon,[†] and Scott A. Gold*[,‡]

[†]Institute for Micromanufacturing, Louisiana Tech University, Ruston, Louisiana 71272, United States

[‡]Chemical and Materials Engineering Department, University of Dayton, Dayton, Ohio 45469, United States

ABSTRACT: Template wetting is simple, solution-based nanofabrication technique that has previously been demonstrated for a number of different polymers. Like other solution-based polymer processing methods, it is reasonable to expect that the choice of solvent will have a significant impact on the properties of the resulting structures. This work examines the impact of wetting solvent on the properties of poly(2-methoxy-5-2′-ethylhexyloxy-1,4-phenylenevinlyene) (MEH-PPV) nanotubules formed using this method. The strength of solvent−polymer interaction was found to positively correspond to the degree of polymer chain alignment in the resulting nanotubules. Alignment was indicated by the level of dichroism observed using polarized FTIR spectroscopy, with no preferential alignment observed when using the poorest solvent (chlorobenzene) and dichroic ratios greater than 10 observed when "good" solvents chloroform and tetrahydrofuran were employed. The degree of alignment in turn correlated to a greater effective conjugation length in the MEH-PPV nanotubules, indicated by a small red shift in the UV−vis absorption band. An even greater impact of solvent on hole mobility was observed, with the best solvent examined yielding a roughly 3 orders of magnitude greater hole mobility than the worst solvent studied in the nanotubules.

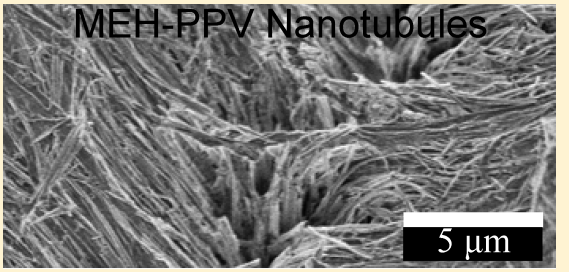

INTRODUCTION

Conjugated polymers such as poly(2-methoxy-5-2′-ethylhexyloxy-1,4-phenylenevinlyene) (MEH-PPV) have shown much promise for electronic device applications.[1−4] Performance of these materials is often limited by poor charge carrier lifetimes and mobilities.[5−8] These and other performance characteristics are strongly related to the molecular order and the degree of interchain π-orbital interaction in the material,[9,10] which is in part a function of the methods and conditions used to fabricate device structures from these polymers as well as of the structure itself. In this work, the impact of wetting solvent in a simple nanofabrication process, template wetting, will be explored.

Polymer molecules in a solid often retain a "memory" of their configuration in solution,[11−13] making solvent choice an important process variable. The conformation of polymer molecules in solution is dependent on the relative strength of solvent−polymer and intrapolymer interaction forces as well as the rotational freedom of bonds making up the polymer chain. Typically, a random coil conformation is thermodynamically favored in solution. In "good" solvents where solvent−polymer interactions dominate, this coil is swollen or enlarged and the polymer chain more stretched or elongated.[14] Conversely, a more tightly coiled conformation where the polymer chain is folded in on itself is favored in "poor" solvents where intrapolymer interaction forces are dominant.[14] Solvents for which these solvent−polymer and intrapolymer foces are in balance and polymer conformation approaches that of an ideal statistical coil are referred to as "theta" solvents.[14] This range of conformations of course presumes sufficient freedom of rotational motion within the polymer chain itself. Little or no solvent dependence on conformation is observed in rigid-rod polymers, planar chain molecules, helically coiled polymers, molecules with side groups that repel one another, and other similar structures.[14] Conjugated polymers may fall into either category. For example, poly(3-hexylthiophene) (P3HT) has been shown to have a relatively rigid structure and a conformation in solution that is largely independent of solvent.[15,16] MEH-PPV, the focus of this work, shows a broad range of potential conformations depending on the solvent.[17] Another solvent-related phenomenon is the formation of aggregates which can occur in poor solvents or at sufficiently high polymer concentrations which can persist in films cast from these solvents.[18] Increased mobility in MEH-PPV spin-cast films from aromatic solvents has been attributed to these aggregates;[18] however, aggregates have been shown to have very different structures depending on the solvent,[17] which might also be expected to be of importance. Solvent effects have also been explained in terms of evaporation rates.[19] Use of high boiling point solvents[20,21] or processing in increased solvent partial pressure in the drying environment[19,20,22] to slow the solvent evaporation rate has been shown to lead to a solvent annealing effect, allowing the polymer chains to arrange in a thermodynamically favorable, generally more ordered orientation with a longer effective conjugation length in the case of conjugated polymers.[11,23] Evaluating the impact of solvent

Received: August 24, 2010
Revised: February 1, 2011
Published: March 04, 2011

choice is complicated by the fact that this impact is highly dependent on the specific process and structure being studied.

Fabrication of nanoscale device structures has been shown to be a promising approach for increasing carrier mobility and controlling the optical properties of conjugated polymers.[24−31] The subject of this work is template wetting, a simple solution-based nanofabrication method relying on surface tension to draw a wetting solution into the nanoscale pores of a template material.[32] This method has been demonstrated as a means controlling the morphology of polymer and liquid crystal materials.[33−35] Polyfluorene nanowires made using this method have also shown chain alignment along with anisotropic luminescence with a preferred axial polarization of wire emission.[36,37] In a previous study, our group observed an order of magnitude increase in mobility and a bathochromic shift in the optical absorption energy of MEH-PPV nanotubules from a chloroform wetting solution as compared to drop-cast films.[38,39]

As template wetting is a solution-based nanofabrication method, the choice of solvent for the wetting solution might be expected to impact on the properties of the resulting polymer nanostructures. However, previous studies of template nanofabrication have attributed increased order in polymers to the high radius of curvature of the nanoscale pores and/or to nanoscale confinement.[32,33,39,40] For this work, the impact of solvent used in the wetting solutions on the spectroscopic and electrical properties of MEH-PPV nanotubules is examined.

MATERIALS AND METHODS

MEH-PPV ($M_{n,avg}$ 70 000−100 000) and ACS reagent grade chlorobenzene (CB), chloroform (CF), tetrahydrofuran (THF), or toluene (TOL) were obtained from Sigma-Aldrich and used as received. Commercially available anodic porous aluminum oxide membranes (Whatman Co.) were used as templates for the nanofabrication process. These were 60 μm thick with nominal pore diameters of 100 nm and 10^{10} pores per cm^2.

A detailed description of the template wetting process can be found elsewhere.[32,38,39,41] In short, a wetting solution is pipetted onto the surface of the template where surface tension allows it to spread over the template surface and penetrate into the pores of the material. The solvent is allowed to evaporate in air overnight leaving behind MEH-PPV nanotubules in the pores. Wetting solutions of the polymer were prepared by dissolution in one of chlorobenzene (CB), chloroform (CF), tetrahydrofuran (THF), or toluene (TOL) at a concentration of 2 mg/mL. Using the bulk density of the polymer and template porosity along with the assumption of cylindrical pores, sufficient solution was added such that the maximum wall thickness of the nanotubles would be 5 nm, i.e., if all polymer penetrated the pores. Excess polymer deposited on the macroscopic outer surfaces of the templates was removed by etching with a 100 W, 200 mTorr helium plasma for 10 min. Short etch times and high pore aspect ratios ensure that the plasma cannot significantly affect the polymer incorporated within the nanoporous membrane. An illustration of the resulting MEH-PPV nanostructures and representative SEM images of the partially released nanotubules removed from the template by etching in aqueous potassium hydroxide are shown in Figure 1.

Thermogravimetric analysis (TGA) was carried out in a TA Instruments Q500 instrument to study solvent evaporation. Wetting solutions with each respective solvent were allowed to evaporate in the nitrogen environment of the TGA at 30 °C until the weight change in the sample was zero. Polymeric solutions typically dry in three stages: an initial rapid weight loss dominated by solvent evaporation, a slower gel drying stage, and a transition region between the two as illustrated in Figure 2. The gel

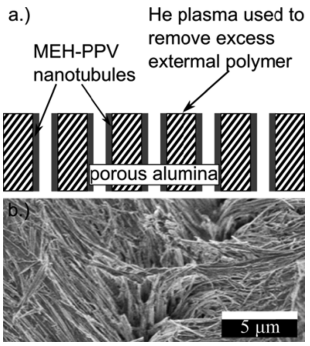

Figure 1. (a) Illustration of MEH-PPV nanotubule structures formed via template wetting, in the template as used for experimental testing. (b) SEM image of an array of nanotubules made using a chloroform wetting solution and partially released from the template to facilitate imaging.

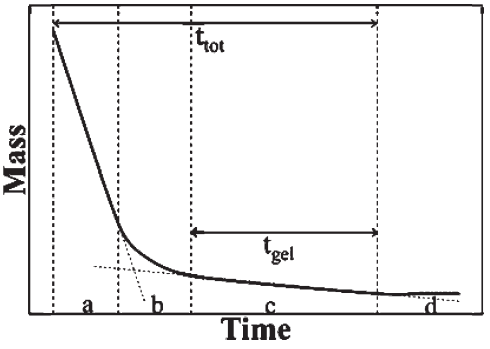

Figure 2. Illustration of typical stages of drying of a polymer solution. An initial rapid solvent evaporation (a) transitions (b) to a slower gel evaporation stage (c) before weight loss ceases, and essentially no solvent remains (d).

Table 1. Ratio of Gel Drying Time to Total Drying Time for P3HT in Various Solvents Determined from TGA

wetting solvent	t_{gel}/t_{tot}
chlorobenzene	0.014
chloroform	0.169
tetrahydrofuran	0.576
toluene	0.052

drying time (t_{gel}) as a fraction of the total drying time (t_{total}) can be taken as a measure of the relative affinity of the solvent for the polymer.[13] If the t_{gel}/t_{total} fraction is the same for two different solvents, then the relative affinity is the same, and the t_{gel} is simply a function of the boiling point of the solvent. Thus, this analysis serves as a way in which to analyze solvent evaporation of a polymeric solution between solvents of differing boiling point.

On the basis of the ratio t_{gel}/t_{total}, the solvents chosen have widely varying interaction with the polymer, with the best solvent being THF, followed in order by chloroform, toluene, and chlorobenzene, as summarized in Table 1. This is consistent with expectations from the literature, where it has been shown that MEH-PPV molecule adopts a more tightly coiled structure in toluene, while straightening to a larger extended coil in chloroform.[42,43] The better solvents are those that interact most strongly with the aliphatic side chains, chloroform and THF, while the poorest solvents interact most strongly with the aromatic rings of the chain backbone.[44−46] The two poorest of these solvents by

this measure, chlorobenzene and toluene, also have the highest boiling points and were the slowest evaporating.

Polarized FTIR spectroscopy is a well-established method for studying the degree of orientation of the polymer chains.[47−49] A Thermo-Nicolet Nexus 470 spectrometer with a slide mount polarizer was employed for this purpose with samples oriented 30° from parallel from the IR beam, as shown in Figure 3, where the intensity of light polarized orthogonal and at 30° to the axes of the nanotubules are $I_\perp$ and I_{30} with absorbances $A_\perp$ and A_{30}, respectively. The parallel polarized absorbance, $A_\parallel$, is a component of the absorbance from the beam labeled I_{30}, which is oriented at an angle of 30° with respect to the tube axis, as described by eq 1.

$$A_{30} = A_\parallel \cos^2(30°) + A_\perp \sin^2(30°) \quad (1)$$

A quantitative measure of chain orientation is the dichroic ratio, R, defined as the ratio of $A_\parallel$ to $A_\perp$. Deviation of this value from unity is indicative of selective orientation of the bond associated with the absorption band. Dividing eq 1 through by $A_\perp$ allows the dichroic ratio to be readily solved for from the measured infrared absorbances, as shown in eq 2.

$$R = \frac{A_\parallel}{A_\perp} = \frac{1}{3}\left(\frac{4A_{30}}{A_\perp} - 1\right) \quad (2)$$

UV−vis spectroscopy was performed using a Shimadzu UV 1650PC spectrometer. Nanotubule samples were analyzed by orienting samples such that the incident beam was normal to the template or film surface. Of particular interest is the energy of the onset of absorption, which corresponds to the optical bandgap or minimum excitation energy required to excite a $\pi-\pi^*$ transition. This value, found from the intersection of the spectrum baseline with a tangent line to the low energy side of the absorption band.

Electronic devices were fabricated by depositing 150 nm thick gold contacts on each side of the templates, forming device structures illustrated in Figure 4. The work function of gold ($\varphi_m \approx 5.1$ eV)[50] is close to the valence band energy of MEH-PPV ($E_V \approx 5.35-5.40$ eV), thus minimizing the hole injection barrier while maximizing the barrier for electrons, ensuring hole only conduction in the devices. Hole mobility was obtained by fitting current−voltage characteristics of these devices, measured with a Keithley 236 source-measure unit, to a general space-charge limited conduction (SCLC) model as is common for conjugated polymers such as MEH-PPV.[8,51] Specifically, data were fit to eq 3, which is a linear combination of low field injection limited ohmic behavior and higher field trap-free SCL conduction

$$J = q\mu_p p \frac{V}{L} + \frac{9}{8}\varepsilon_0\varepsilon_r\mu_p\frac{V^2}{L^3} \quad (3)$$

where V is the applied voltage, $\varepsilon_0\varepsilon_r$ is the electrical permittivity of the material, μ_p is the hole mobility, L is the device length, and p is free carrier concentration in the material before space-charge accumulation becomes important.[51−55] Expressing this model in the form of a simple power series

$$J = aV^2 + bV \quad (4)$$

allows mobility to be found directly from a. Device length is equivalent to the template thickness of 60 μm while device area was roughly and conservatively estimated to be the cross-sectional area of a cylinder with an outer diameter equal to the pore diameter (100 nm) and wall thickness of 5 nm (the upper bound based on the amount of polymer used) multiplied by the pore density and geometric area of the device. The value of ε_r was taken to be 3, which is commonly done for PPVs.[8]

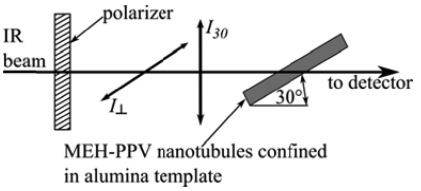

Figure 3. Illustration of sample orientation for polarized spectroscopy.

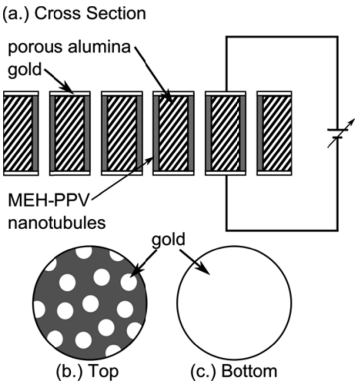

Figure 4. Illustration of devices used for measurement of hole mobility of MEH-PPV in nanotubules shown in cross section (a). Multiple gold contacts were evaporated through a shadow mask on the top (b) and a single large contact over the entire back of each sample (c), allowing for hole only conduction and multiple devices per sample.

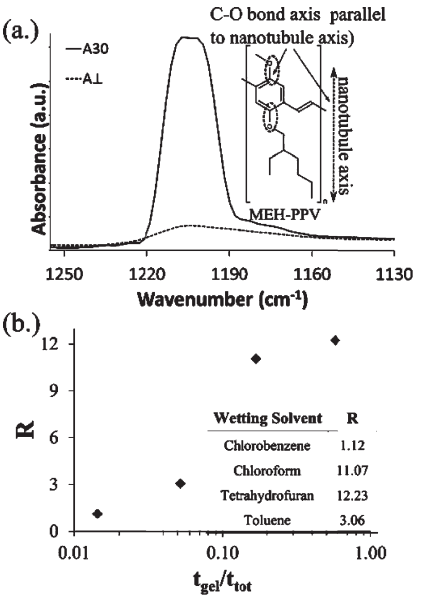

Figure 5. (a) FTIR absorption band associated with the C−O stretch (shown in the inset to the right) collected with ⊥ and 30° polarized light for P3HT nanotubules cast from chloroform. (b) Dichroic ratios (R) calculated for this and other solvents tested are plotted vs t_{gel}/t_{tot} for each respective solvent, with values given in the lower right.

RESULTS AND DISCUSSION

Polarized FTIR. FTIR spectra of 100 nm nanotubules of MEH-PPV are shown for the ⊥ and 30° polarization states in Figure 5a, focusing on the vibrational band at ∼1210 cm^{-1}. This

band is associated with the C−O stretch of the methoxy and/or ethylhexyloxy side chains extending from the phenyl ring, highlighted in the inset of Figure 5a.[56] The dichroic ratio, R, calculated using eq 2, correlates with the quality of solvent as measured by the ratio t_{gel}/t_{total} and shown in Figure 5b. The large values of R for the two good solvents, CF and THF, indicate preferential alignment of the C−O bond axis parallel to the axis of the nanotubules while little or no alignment of the polymer chains is seen in samples prepared using TOL or CB. As noted previously, the nonaromatic solvents interact most strongly with the aliphatic side chain of the polymer.[44−46] That being the case, one would expect the side chains to be extended away from the conjugated backbone in these "good" solvents, which helps explain the observed preferential alignment of the C−O bond at the base of these molecular appendages.

Previous studies had attributed molecular order observed in template fabricated nanostructures primarily to curvature-induced crystallization or nanoscale confinement with greater order observed as the pore diameter in the template decreased.[32,33,39,40] The influence of solvent shown here indicates a somewhat more complex mechanism. We can speculate that the observed molecular order in this and other template fabricated structures is the result of the relative influence of the various forces acting on the polymer molecules. The template−polymer interactions would include a compression like force imparted by the radius of curvature mentioned previously as well as surface interactions responsible for the wetting effect and tubule formation observed in this work as well as the effect of alignment substrates, such as those employed by Sirringhaus et al.[10] or of variations across the film thickness in spin-cast films.[57] Solvent−polymer interactions would include an extrusion-like effect due to surface tension as the solvent evaporates and liquid meniscus proceeds down the pore. A similar mechanism has been suggested to explain crystal domains observed in single conjugated polymer droplets and inkjet deposited films.[57] The "memory" of the polymer conformation in solution should also have an impact. Using this same nanofabrication process, the impact of solvent was observed to be much more modest on molecular alignment in nanotubules of poly(3-hexylthiophene) (P3HT), a rigid-rod polymer with far less conformational variation in different solvents than MEH-PPV.[58]

Electronic Spectra. UV−vis spectra, focusing on the absorption band shown associated with the $\pi-\pi^*$ transition, are displayed in Figure 6a for 100 nm MEH-PPV nanotubules fabricated from chlorobenze, chloroform, tetrahydrofuran, and toluene solutions. Spectra from the "good" solvents, tetrahydrofuran and chloroform, are different from those of the "poor" solvents. The minimum excitation energy for a $\pi-\pi^*$ transition, or the optical bandgap energy (E_g), is red-shifted in the "good" solvents, to ∼2.00 eV from ∼2.05 eV in the two "poor" solvents.

Further differences are illuminated by taking to mathematical derivatives of the spectra to reveal constituent peaks of the of the absorption bands. The constituent peaks, all associated with the $\pi-\pi^*$ transition associated with different molecular arrangements, were found from the minima in the second derivative and maxima in the fourth derivative of the spectra, as shown in Figure 7. While much work has been done to associate different absorption energies with molecular arrangements in solution,[59] this does not directly translate to solids with a more complex band structure, making it difficult to assign UV−vis peaks to any specific molecular arrangement. The primary difference observed in the fine structure of the absorption bands is the presence of an

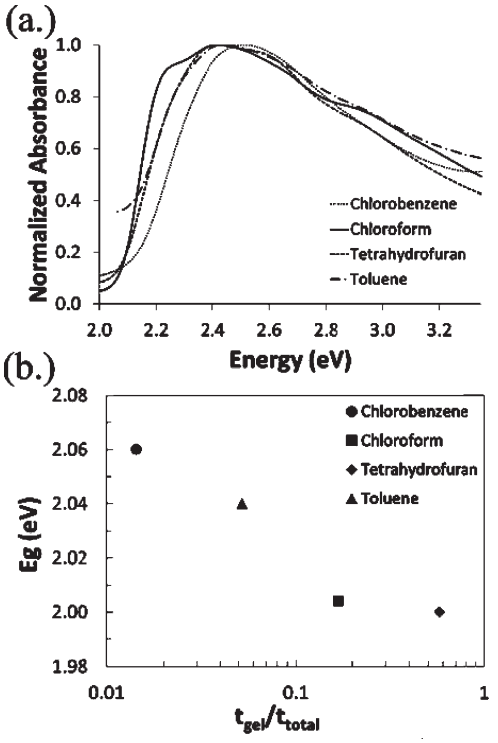

Figure 6. (a) UV−vis absorbance bands associated with the $\pi-\pi^*$ transition in 100 nm MEH-PPV nanotubules made using different wetting solvents. (b) Energy of the optical bandgap (E_g) or onset of absorption plotted vs t_{gel}/t_{total}.

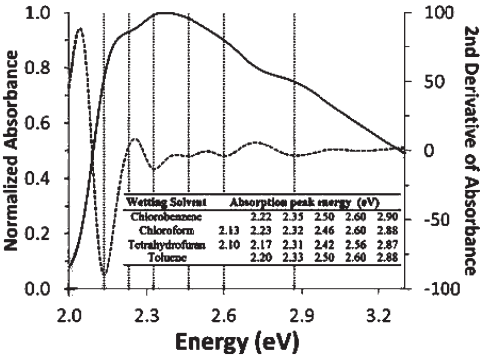

Figure 7. UV−vis spectrum (solid curve) and second derivative (dashed curve) for 100 nm MEH-PPV nanotubles made using chloroform. Minima in this and maxima in the fourth derivative (vertical dashed lines) were used to identify constituent peak energies of the UV−vis absorbance bands associated with the $\pi-\pi^*$ nanotubules made using different wetting solvents, listed in the inset table.

additional low-energy peak at ∼2.10 eV in the nanotubules made using the nonaromatic chloroform and tetrahydrofuran wetting solvents, providing a further means of describing the red shift of the band. In general, lower absorbance energies are associated with longer effective conjugation lengths and greater molecular order in the polymer.[44]

Electrical Characterization. Representative current density−voltage data from devices illustrated in Figure 4 along with regression fit curves to eq 3 are shown in Figure 8a. The strong wetting solvent dependence is readily apparent and consistent

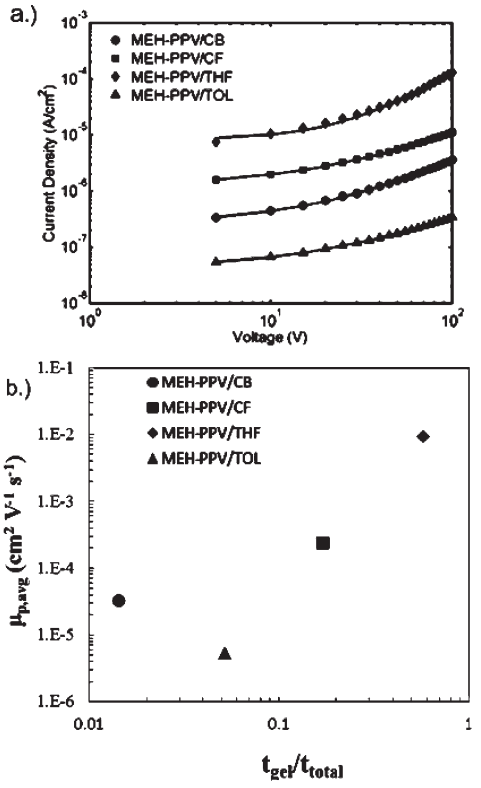

Figure 8. (a) Representative current density−voltage plots for MEH-PPV nanotubules cast from different solvents. (b) Mobility of those nanotubules as a function of the t_{gel}/t_{tot}.

with expectations from previously presented data. The two best solvents, tetrahydrofuran and chloroform, yielded nanostructures with hole mobilities 2−3 orders of magnitude greater than those with the two poorer solvents, chlorobenzene and toluene, as shown in Figure 8b. The nanotubules made from toluene wetting solutions appear not to conform to the trend of corresponding to the degree of alignment indicated by the dichroic ratio of the C−O stretching vibration with a mobility slightly lower than that of the nanotubules made with the marginally poorer solvent, chlorobenzene. We speculate that this might be accounted for by a small difference in nanotubule wall thickness caused by differences in the surface tension of the wetting solutions. As previously noted, the wall thickness was conservatively estimated to be 5 nm, which assumed that all polymer applied to the templates contributed to nanotubule formation. The impact of small differences in wall thickness and hence active device area would be magnified at the low carrier mobility levels observed with the two poorer solvents.

The trend in mobility observed here is counter to that observed in other studies. Using this same process with P3HT, no significant solvent dependence on mobility was observed, though a similar if more much more modest trend was observed in alignment and the onset of UV−vis absorption.[58] This is likely because conformation of amorphous MEH-PPV varies much more with solvent than that of rigid-rod P3HT. Geens et al. looked at solvent effects in a in spin-cast films of a similar polymer, poly(2-methoxy-5-(30,70-dimethyloctyloxy)-1,4-phenylenevinylene) (MDMO-PPV), and observed an ∼1 order of magnitude increase in mobility in the poorer aromatic solvents (chlorobenzene and toluene) than in nonaromatic THF and CF, from 10^{-6} to 10^{-5} $cm^2/(V\ s)$.[18] This was attributed to the formation of aggregates in solution that persisted into the spun-cast films with a reduced the barrier to interchain transport.[18] In a similar result, Liu et al. when examining a photovoltaics constructed with spin-cast MEH-PPV and buckminsterfullerene from different solvents observed that nonaromatic solvents (THF and CF) yielded devices that exhibited a smaller photocurrent and higher open-circuit voltage.[46] This was attributed to the extension of the side chains preventing intimate contact between the conjugated backbone of the polymer and the buckminsterfullerene.[46] Different trends in these studies from results reported here can be attributed to the very different device structure and fabrication process. Curvature-induced molecular order and surface tension forces during nanotubule formation as well forces imparted by the curvature of the porous template, discussed previously, are absent in spin-cast films. These forces led to much higher mobilities as much as 4 orders of magnitude higher than typically observed in thin films of MEH-PPV.[60] Also, unlike the single carrier devices described here, mobility in devices fabricated by Liu et al. was limited by electron transfer from the MEH-PPV to the buckminsterfullerene.

CONCLUSIONS

Solvent quality plays a strong role in determining properties of MEH-PPV nanotubules formed via template wetting. Previous studies of template wetting of polymers had attributed increased molecular order and other changes in material properties primarily to curvature-induced effects or confinement in the nanoscale. Results reported here reveal a more complex mechanism in which the solvent plays a key role. Solvent affinity toward the polymer determined from the ratio of the gel evaporation time to the total evaporation time of the solution was found to correspond to a greater degree of polymer chain alignment in nanotubules. This in turn was found to lead to greater effective conjugation lengths in the polymer, as observed in the UV−vis spectra, and higher carrier mobilities. In contrast, the solvents with the highest boiling points that yielded the slowest evaporating solutions, toluene and chlorobenzene, yielded nanotubules with the least degree of chain alignment, shortest effective conjugation lengths, and lowest carrier mobilities. It can thus be concluded that the orientation of the polymer chain in solution is of greater consequence than any solvent annealing or evaporation rate effect for template wetting, at least for the amorphous MEH-PPV polymer examined here. Interestingly, while the choice of wetting solution had a strong influence on the orientation and properties of MEH-PPV nanotubules, this process parameter had a much more limited impact when using a different conjugated polymer, poly(3-hexylthiophene) (P3HT). Unlike amporphous MEH-PPV, P3HT is semicrystalline and assumes a rigid-rod conformation in solution, thus limiting any solvent impact. The "good" solvents in this case interacted most strongly with the aliphatic side chains of the MEH-PPV, resulting in an in enlarged polymer coil in solution. We speculate that, in addition to this effect, surface tension during evaporation in conjunction with confinement in the template pores acted to induce preferential alignment of the polymer chains in the resulting nanotubules with carrier mobilites as much as 4 orders of magnitude greater than observed in thin films. The absence of these effects resulted in opposite trends in carrier mobility being reported in thin films.

AUTHOR INFORMATION

Corresponding Author

*Tel +1 937 229-2977; fax +1 937 229-3433; e-mail Scott.Gold@notes.udayton.edu.

REFERENCES

(1) Shaw, J. M.; Seidler, P. F. *IBM J. Res. Dev.* **2001**, *45* (1), 3–8.
(2) Braun, D.; Heeger, A. J. *Appl. Phys. Lett.* **1991**, *58* (18), 1982–4.
(3) Yu, G.; Zhang, C. *Appl. Phys. Lett.* **1994**, *64* (12), 1540–1542.
(4) Granstrom, M.; Petritsch, K.; Arias, A. C.; Lux, A.; Andersson, M. R.; Friend, R. H. *Nature* **1998**, *395* (6699), 257–260.
(5) Dimitrakopoulos, C. D.; Mascaro, D. J. *IBM J. Res. Dev.* **2001**, *45* (1), 11–27.
(6) Forrest, S. R. *Nature* **2004**, *428* (6986), 911–918.
(7) Chen, Y.-S.; Meng, H.-F. *Phys. Rev. B* **2002**, *66* (3), 035202.
(8) Blom, P. W. M.; de Jong, M. J. M.; Vleggaar, J. J. M. *Appl. Phys. Lett.* **1996**, *68* (23), 3308–3310.
(9) Sirringhaus, H.; Brown, P. J.; Friend, R. H.; Nielsen, M. M.; Bechgaard, K.; Langeveld-Voss, B. M. W.; Spiering, A. J. H.; Janssen, R. A. J.; Meijer, E. W.; Herwig, P.; de Leeuw, D. M. *Nature* **1999**, *401* (6754), 685–688.
(10) Sirringhaus, H.; Wilson, R. J.; Friend, R. H.; Inbasekaran, M.; Wu, W.; Woo, E. P.; Grell, M.; Bradley, D. D. C. *Appl. Phys. Lett.* **2000**, *77* (3), 406–408.
(11) Bao, Z.; Dodabalapur, A.; Lovinger, A. J. *Appl. Phys. Lett.* **1996**, *69* (26), 4108.
(12) Schwartz, B. J. *Annu. Rev. Phys. Chem.* **2003**, *54* (1), 141–172.
(13) Lee, S.; Lee, J. Y.; Lee, H. *Synth. Met.* **1999**, *101* (1), 248–249.
(14) Grulke, E. A. *Polymer Process Engineering*; Prentice Hall: Englewood Cliffs, NJ, 1994.
(15) Pal, S.; Nandi, A. K. *J. Appl. Polym. Sci.* **2006**, *101* (6), 3811–3820.
(16) Heffner, G. W.; Pearson, D. S. *Macromolecules* **1991**, *24* (23), 6295–6299.
(17) Traiphol, R.; Charoenthai, N.; Srikhirin, T.; Kerdcharoen, T.; Osotchan, T.; Maturos, T. *Polymer* **2007**, *48* (3), 813–826.
(18) Geens, W.; Shaheen, S. E.; Wessling, B.; Brabec, C. J.; Poortmans, J.; Sariciftci, N. S. *Org. Electron.* **2002**, *3* (3−4), 105–110.
(19) Li, G.; Yao, Y.; Yang, H.; Shrotriya, V.; Yang, G.; Yang, Y. *Adv. Funct. Mater.* **2007**, *17* (10), 1636–1644.
(20) Kline, R. J.; McGehee, M. D.; Kadnikova, E. N.; Liu, J.; Frechet, J. M. J.; Toney, M. F. *Macromolecules* **2005**, *38* (8), 3312–3319.
(21) Chang, J.-F.; Clark, J.; Zhao, N.; Sirringhaus, H.; Breiby, D. W.; Andreasen, J. W.; Nielsen, M. M.; Giles, M.; Heeney, M.; McCulloch, I. *Phys. Rev. B* **2006**, *74* (11), 115318.
(22) Do Hwan, K.; Yeong Don, P.; Yunseok, J.; Sungsoo, K.; Kilwon, C. *Macromol. Rapid Commun.* **2005**, *26* (10), 834–839.
(23) Nguyen, T. Q.; Doan, V.; Schwartz, B. J. *J. Chem. Phys.* **1999**, *110* (8), 4068–4078.
(24) Li, D.; Babel, A.; Jenekhe, S. A.; Xia, Y. *Adv. Mater.* **2004**, *16* (22), 2062–2066.
(25) Aryal, M.; Buyukserin, F.; Mielczarek, K.; Zhao, X. M.; Gao, J.; Zakhidov, A.; Hu, W. *J. Vac. Sci. Technol., B: Microelectron. Nanometer Struct.* **2008**, *26* (6), 2562–2566.
(26) Aryal, M.; Trivedi, K.; Hu, W. *ACS Nano* **2009**, *3* (10), 3085–3090.
(27) Cheyns, D.; Vasseur, K.; Rolin, C.; Genoe, J.; Poortmans, J.; Heremans, P. *Nanotechnology* **2008**, *19* (42), 424016.
(28) De Marco, C.; Mele, E.; Camposeo, A.; Stabile, R.; Cingolani, R.; Pisignano, D. *Adv. Mater.* **2008**, *20* (21), 4158–4162.
(29) Martin, C. R. *Science (Washington, D.C.)* **1994**, *266* (5193), 1961–6.
(30) Liang, W.; Martin, C. R. *J. Am. Chem. Soc.* **1990**, *112* (26), 9666–9668.
(31) O'Brien, G. A.; Quinn, A. J.; Tanner, D. A.; Redmond, G. *Adv. Mater.* **2006**, *18* (18), 2379–2383.
(32) Steinhart, M.; Wendorff, J. H.; Wehrspohn, R. B. *ChemPhysChem* **2003**, *4* (11), 1171–1176.
(33) Steinhart, M.; Senz, S.; Wehrspohn, R. B.; Gosele, U.; Wendorff, J. H. *Macromolecules* **2003**, *36* (10), 3646–3651.
(34) Steinhart, M.; Wendorff, J. H.; Greiner, A.; Wehrspohn, R. B.; Nielsch, K.; Schilling, J.; Choi, J.; Goesele, U. *Science* **2002**, *296* (5575), 1997.
(35) Steinhart, M.; Zimmermann, S.; Goring, P.; Schaper, A. K.; Gosele, U.; Weder, C.; Wendorff, J. H. *Nano Lett.* **2005**, *5* (3), 429–434.
(36) O'Carroll, D.; Redmond, G. *Phys. E* **2008**, *40* (7), 2468–2473.
(37) O' Carroll, D.; Irwin, J.; Tanner, D. A.; Redmond, G. *Mater. Sci. Eng., B* **2008**, *147* (2−3), 298–302.
(38) Cannon, J. P.; Bearden, S. D.; Gold, S. A. *Composites, Part A* **2010**, *41* (7), 836–841.
(39) Cannon, J. P.; Bearden, S. D.; Khatkhatay, F. M.; Cook, J.; Selmic, S. Z.; Gold, S. A. *Synth. Met.* **2009**, *159* (17−18), 1786–1791.
(40) Duvail, J. L.; Retho, P.; Fernandez, V.; Louarn, G.; Molinie, P.; Chauvet, O. *J. Phys. Chem. B* **2004**, *108* (48), 18552–18556.
(41) Steinhart, M.; Wendorff, J. H.; Greiner, A.; Wehrspohn, R. B.; Nielsch, K.; Schilling, J.; Choi, J.; Gosele, U. *Science* **2002**, *296* (5575), 1997.
(42) Lee, C. K.; Hua, C. C.; Chen, S. A. *J. Phys. Chem. B* **2008**, *112* (37), 11479–11489.
(43) Huser, T.; Yan, M.; Rothberg, L. J. *Proc. Natl. Acad. Sci. U.S.A.* **2000**, *97* (21), 11187–11191.
(44) Zheng, M.; Bai, F.; Zhu, D. *J. Photochem. Photobiol., A* **1998**, *116* (2), 143–145.
(45) Amrutha, S. R.; Jayakannan, M. *J. Phys. Chem. B* **2008**, *112* (4), 1119–1129.
(46) Liu, J.; Shi, Y. J.; Yang, Y. *Adv. Funct. Mater.* **2001**, *11* (6), 420–424.
(47) Zbinden, R. *Infrared Spectroscopy of High Polymers*; Academic Press: New York, 1964.
(48) Parthasarathy, R. V.; Martin, C. R. *Chem. Mater.* **1994**, *6* (10), 1627–1632.
(49) Jasse, B.; Koenig, J. L. *J. Macromol. Sci., Rev. Macromol. Chem.* **1979**, *C17* (1), 61–135.
(50) Campbell, I. H.; Hagler, T. W.; Smith, D. L.; Ferraris, J. P. *Phys. Rev. Lett.* **1996**, *76* (11), 1900.
(51) Antoniadis, H.; Abkowitz, M. A.; Hsieh, B. R. *Appl. Phys. Lett.* **1994**, *65* (16), 2030.
(52) Lampert, M. A. *Phys. Rev.* **1956**, *103* (6), 1648.
(53) Chiguvare, Z.; Parisi, J.; Dyakonov, V. *J. Appl. Phys.* **2003**, *94* (4), 2440–2448.
(54) Chirvase, D.; Chiguvare, Z.; Knipper, M.; Parisi, J.; Dyakonov, V.; Hummelen, J. C. *Synth. Met.* **2003**, *138*, 299–304.
(55) Mott, N. F.; Gurney, R. W. *Electronic Processes in Ionic Crystals*, 2nd ed.; Oxford University Press: New York, 1948; p 274.
(56) Scott, J. C.; Kaufman, J. H.; Salem, J.; Goitia, J. A.; Brock, P. J.; Dipietro, R. *Mol. Cryst. Liq. Cryst. Sci. Technol., Sect. A* **1996**, *283*, 57–62.
(57) Wong, L. Y.; Png, R. Q.; Silva, F. B. S.; Chua, L. L.; Repaka, D. V. M.; Shi, C.; Gao, X. Y.; Ke, L.; Chua, S. J.; Wee, A. T. S.; Ho, P. K. H. *Langmuir* **2010**, *26* (19), 15494–15507.
(58) Cannon, J. P.; Bearden, S. D.; Gold, S. A. *Synth. Met.* **2010**, *160* (23−24), 2623–2627.
(59) Palsson, L.-O.; Vaughan, H. L.; Monkman, A. P. *J. Chem. Phys.* **2006**, *125* (16), 164701/1–164701/7.
(60) Campbell, I. H.; Smith, D. L.; Neef, C. J.; Ferraris, J. P. *Appl. Phys. Lett.* **1999**, *75* (6), 841–843.